Journal of Electroanalytical Chemistry 971 (2024) 118591

Contents lists available at ScienceDirect

Journal of Electroanalytical Chemistry

journal homepage: www.elsevier.com/locate/jelechem

A versatile electrochemical cell for *in-situ* GI-XRD measurements on lab-scale XRD devices

Fabian Froech [a], Sabine Kubicek [b], Werner Artner [a], Michael Nelhiebel [b], Silvia Larisegger [c], Guenter Fafilek [a,*]

[a] *Institute of Chemical Technologies and Analytics, TU Wien, Getreidemarkt 9/164ec, 1060 Vienna, Austria*
[b] *KAI Kompetenzzentrum Automobil-und Industrieelektronik GmbH, Europastraße 8, 9524 Villach, Austria*
[c] *KAI Kompetenzzentrum Automobil-und Industrieelektronik GmbH, Argentinierstraße 8, 1040 Vienna, Austria*

ARTICLE INFO

Keywords:
In-situ X-ray diffraction
Galvanic deposition
Thin film
Electrode surface

ABSTRACT

In-situ X-ray diffraction (XRD) cells for electrochemical experiments suffer from strong attenuation of primary and diffracted beams within the electrolyte solution. To reduce the intensity loss of the X-rays, the use of a thin layer of electrolyte solution is an essential element of the conventional cell design. On the other hand, the thin layer electrolyte geometry is a considerable limitation for electrochemical measurements. To overcome these drawbacks a versatile electrochemical cell for in-situ GI-XRD measurements was constructed and used for the electrodeposition of Cu_2O thin films on a copper substrate.

In this design, a thin copper metal film working electrode is applied on a polyimide foil and then backside-illuminated in GI-XRD geometry. In this way, the XRD pattern is measured from the electrolyte/electrode interface of the working electrode. The X-rays only have to penetrate the polymer foil and the sputtered metal layer, resulting in high-intensity signals.

In this work, we demonstrate the abilities of the *in-situ* cell with quantitative measurements of cathodic deposition of Cu_2O thin layers. The results show a good agreement between the diffracted X-ray peak intensities and the calculated and measured thicknesses of the oxide layers. The cell design allows the structural characterization of electrode surfaces during electrochemical measurements without the disadvantages of thin layer cells and therefore does not require high intensity synchrotron radiation to perform X-ray diffraction during electrochemical investigations.

1. Introduction

X-ray diffraction is employed to acquire a deeper understanding of structural changes during electrochemical reactions, such as phase composition or growth orientation. Structural analysis is typically conducted through *ex-situ* methods. However, changing the environment or a time delay between processing and analysis can lead to potential alterations in material structure or chemical composition [1]. Therefore, the electrochemical reactions involving charge and discharge of battery electrodes, deposition, dissolution, or corrosion are best analyzed during the process [2]. *In-situ* low-angle XRD techniques prove particularly suitable for investigating electrode/electrolyte interfaces, allowing for the direct detection of reaction products [3]. This capability is especially critical when dealing with short-lived and oxygen-sensitive products [4]. For these reasons, *in-situ* techniques are of outstanding importance in electrochemistry research. They offer precise, real-time monitoring of electrode reactions, the charging and discharging processes of batteries, and structural changes in electrode materials. *In-situ* methods provide crucial insights for optimizing electrochemical systems, thereby contributing to the development and enhancement of energy-efficient technologies. One noteworthy *in-situ* technique is grazing incidence X-ray Diffractometry (GI-XRD), a specialized method with high surface sensitivity to investigate thin films. Employed in materials science, GI-XRD utilizes a low incidence angle to enhance the characterization of near-surface structures [5,6].

Water is strongly absorbing the beam from the commonly used Cu K-α source. Therefore, regular cell designs with relatively large solution volumes are not suitable for such measurements. As an example, according to Equation (1), the relation between the remaining intensity I and initial intensity of the beam I_0 after transmission through a 1 cm

---

[*] Corresponding author.
E-mail address: guenter.fafilek@tuwien.ac.at (G. Fafilek).

https://doi.org/10.1016/j.jelechem.2024.118591
Received 7 June 2024; Received in revised form 16 August 2024; Accepted 18 August 2024

thick aqueous solution is in the range of $4.54 \cdot 10^{-5}$. The value for $\mu/\rho \simeq 10\ \mathrm{cm}^2\ \mathrm{g}^{-1}$ has been taken from NIST [7], d is the thickness of the solution in cm and ρ the density of water in g cm^{-3}.

$$\frac{I}{I_0} = exp^{-\frac{\mu}{\rho}\cdot(d\cdot\rho)} \tag{1}$$

In the late 90s, a team led by Fleischmann presented for the first time an *in-situ* X-ray diffraction cell, suitable for transmission and reflection mode measurements. The cell contained a working electrode covered by a Mylar® film as a transparent window material penetrated by the X-rays. To increase signal intensities, the electrolyte volume between the working electrode and the window should be as small as possible [8]. Despite the thin electrolyte solution layer in the range of hundreds of μm, the beam absorption remains high at low incidence angles in reflection mode. As mentioned, grazing incidence setups are applied for investigating thin films. Therefore, most *in-situ* XRD cells use synchrotron radiation to guarantee high signal intensities [9,10]. Some issues occurring by the limited cell volume are the inhomogeneous current density distribution due to the non-optimal position of the counter electrode and a considerable ohmic voltage drop caused by the large distance of the reference to the working electrode. Beyond that the electrolyte layer between the working electrode and the Mylar® film enables only low current densities caused by its resistance. To further refine *in-situ* cells a conductive X-ray transparent window was employed. The conductive window acts as the counter electrode, and the working electrode can be positioned parallel to the counter electrode [11,12]. It is important to ensure that the counter electrode is not placed too close to the working electrode because products formed at the counter electrode might migrate to the working electrode and react there, which would be a significant issue. Furthermore, the small electrolyte volume above the working electrode leads to quick depletion of reactants and does not allow efficient convection.

Another challenge is to decrease the voltage drop inside the thin solution layer. One proposed solution was directly integrating the working electrode material onto an X-ray permeable window. With this approach higher signal intensities can be achieved as the beam does not penetrate a liquid layer. In addition, the design allows the use of an electrolyte volume of any size reducing the effects of depleting mass transport [13]. Similar principles influenced the design of this *in-situ* XRD cell [14]. However, instead of crossing the electrolyte solution, the X-ray must pass a thin layer of the current collector material. The thickness of this metal electrode plays a decisive role: (i) not be too thick to avoid beam absorption; (ii) not be too thin to avoid voltage drop in the film at high current densities. For the given geometry, the influence of the sheet resistance on the current density distribution is estimated.

For investigating the functionality of our *in-situ* GI-XRD cell design an established process for set-up checks is advantageous. The cuprous oxide deposition from a copper lactate system is well described in the literature [15]. It is a non-toxic, easily processable, and cheap metal in the semiconductor and solar industry [5]. Solar cells with p-type Cu_2O could reach a theoretical efficiency of about 20 % [16]. The specific model reaction chosen is the electrochemical deposition of copper oxide from an alkaline copper lactate solution. Cu^{2+} ions are not stable in aqueous solutions at high pH values, therefore a complexing agent is required [17]. The Cu^{2+} ion is surrounded by four lactate ions, acting as the complexing agent, to inhibit the formation of $Cu(OH)_2$. The formed copper(II)lactate complex is stable in a wide range of pH values [18]. When the Cu^{2+} ion is reduced to Cu^{+} the complex decomposes and Cu_2O forms. Overall, the galvanostatic electrodeposition mechanism consists of two steps: reducing Cu^{2+} ions and the precipitation of Cu^{+} ions to molecules of Cu_2O on the working electrode [16].

Electrochemical deposition allows the control of structure, thickness, or stoichiometry of copper oxide films by adjusting parameters like pH, temperature, current density, or time [19]. Upon closer examination, the deposition rate in galvanostatic deposition remains constant, ensuring uniform film thicknesses up to 2 μm [15]. In addition to the galvanostatic deposition, the copper–water system covers three additional reaction mechanisms at distinct pH values and potentials. The Pourbaix diagram provides a comprehensive visualization of the various phases within the copper–water system, involving the following four reactions: anodic dissolution of Cu and cathodic deposition of Cu at low pH, cathodic deposition of Cu_2O, and anodic conversion to Cu_2O at high pH [20]. By modifying parameters, precise control over these reactions is achievable. Consequently, the copper–water system proves to be an ideal model for evaluating the functionality of the designed *in-situ* GI-XRD cell. As mentioned earlier, the third case involving the cathodic galvanostatic deposition of Cu_2O was selected.

2. Cell design and construction

Fig. 1 shows on the left the scheme of a conventional setup of an *in-situ* GI-XRD cell. The X-rays must pass through the electrolyte before reaching the working electrode surface. X-ray intensity is considerably lost if the gap between the polymer foil and the working electrode is too big. As mentioned in the introduction, the thin electrolyte film in a small gap leads to a number of problems that limit the functionality of a galvanic cell. Therefore, most approaches used synchrotron radiation to get appropriate intensities.

The proposed solution here is the cell geometry depicted on the right in Fig. 1. The construction drawing in Fig. 2 presents our proposal for a versatile *in-situ* GI-XRD cell. In our example, a sputtered copper layer onto a polymer foil serves as the working electrode. The low-angle beam penetrates through the back side of the copper layer and isn't attenuated by the solution. Higher intensities are achieved since the thin polymer foils have lower X-ray absorption than the electrolyte layer in the conventional setup. The X-ray also penetrates the copper coating and reaches the electrode-solution interface. Galvanic deposits, such as copper oxide or copper, are detected directly at the phase boundary with minimal loss of intensity (see Fig. 3).

Moreover, the cell design favors the positioning of the reference and counter electrode. The reference electrode is close to the working electrode, which reduces the ohmic drop. The geometry of the cell is customizable, without restrictions on the size and position of the counter electrode. Here, the parallel placement of the counter electrode to the polymer foil results in a homogeneous current density distribution. Consequently, a unique feature of this setup is the possibility of performing measurements with high current densities. Additionally, access to an external electrolyte reservoir can be installed, and electrolyte circulation can be controlled. It is possible to dimension the electrolyte volume to any size, apply forced convection, and thus eliminate the effects of depletion of electroactive species and restricted diffusion.

The cell is a cylindrical body of polyether ether ketone (PEEK). It measures 25 mm in inner diameter, 30 mm in height, and has four ports. The openings can be used for installing the reference electrode (Ag|AgCl), counter electrode (Cu), and the inlet and outlet of the electrolyte solution. The working electrode consists of a Mylar® foil (7.5 μm) with a sputtered-on 1 μm copper layer. An aluminum ring and six screws secure the foil at the cell body and an O-ring prevents leakage. Between the working electrode and the cell outside the O-ring, a thin copper ring is inserted to contact the working electrode during measurements.

To estimate the ohmic voltage drop within the thin metal film which might influence the primary current density distribution across the electrode surface, a simulation with the network method for electrical circuits with the free circuit simulation software LTspice® [21] was performed. A two-dimensional resistor network representation of the cylinder-symmetric cell was developed for that purpose.

3. Experimental

For polarization during *in-situ* X-ray diffraction measurements, an Autolab potentiostat/galvanostat PGSTAT101 is utilized and placed

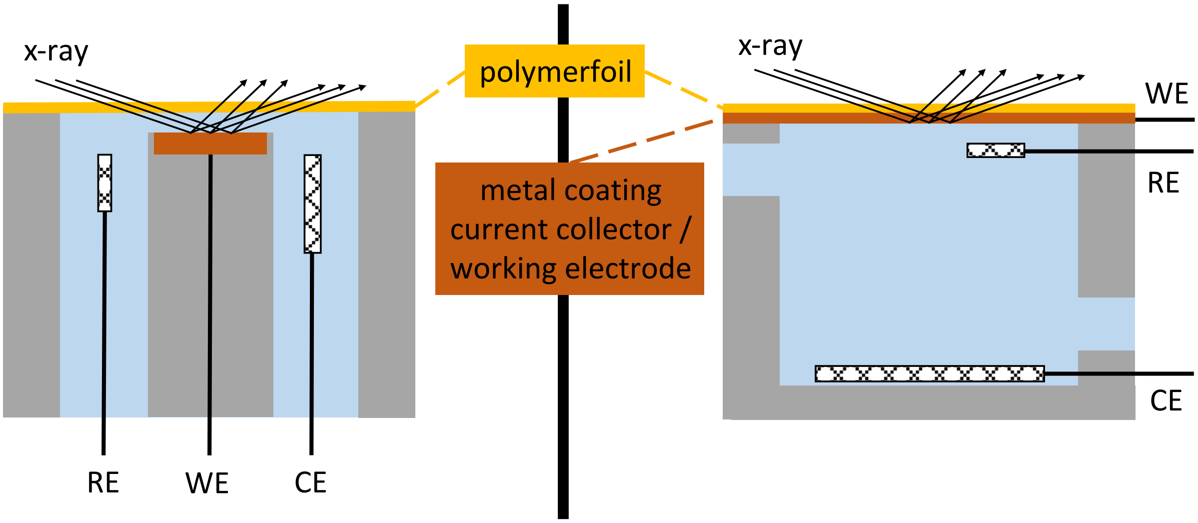

Fig. 1. Left: scheme of a conventional setup of an *in-situ* cell; Right: scheme of our proposed *in-situ* GI-XRD cell geometry.

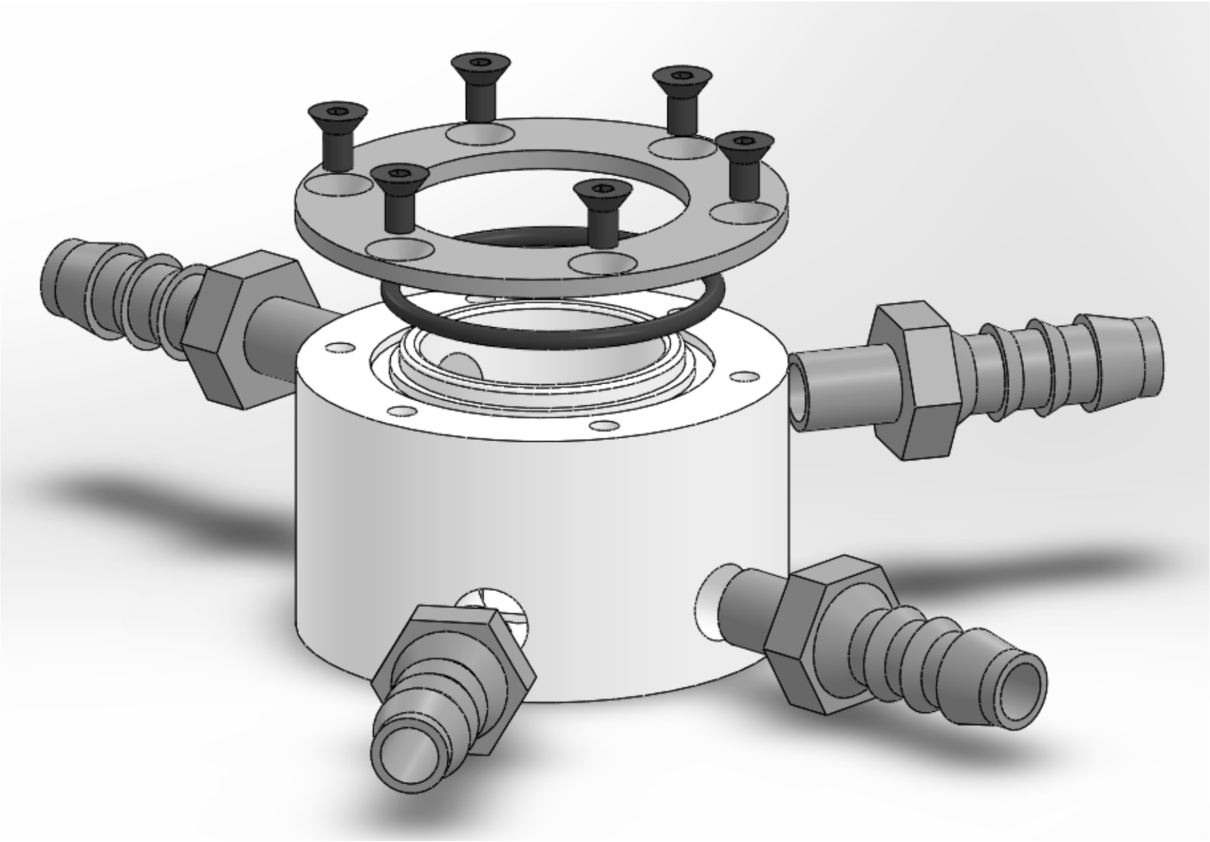

Fig. 2. Visual construction of the *in-situ* GI-XRD cell [14]. © The Electrochemical Society. Reproduced by permission of IOP Publishing. All rights reserved.

outside the diffractometer. Customized cables guarantee electrical connections with the electrodes within the measuring cell. The PANalytical Empyrean XRD diffractometer is used for the XRD-measurements, with all measurements performed exclusively using the grazing incidence mode. Cu K-α radiation, with a wavelength of 1.54 Å, is used as a radiation source. An optimal measurement configuration is achieved using a 1/4° divergence slit and a 4 mm mask.

Concerning the XRD measurements, a constant grazing incidence angle is directed toward the sample, while the detector executes a circular path around the specimen holder. The optimum incidence angle for our cell geometry and copper layer thickness was determined by multilayer calibration. In the multilayer calibration, different metals are sputtered on the foil. To obtain high signal intensities from the surface of the working electrode, the investigation proposed an ideal value of 3° [14]. Before and following to the electrochemical measurements, a comprehensive diffraction pattern, covering 2θ values ranging from 10 to 120°, is recorded. For *in-situ* measurements, the angular range is constrained to the relevant interval of 35–45°. These specific angles are selected due to their correspondence to the dominance of Cu and Cu_2O peaks, allowing for a thorough evaluation of the deposition process.

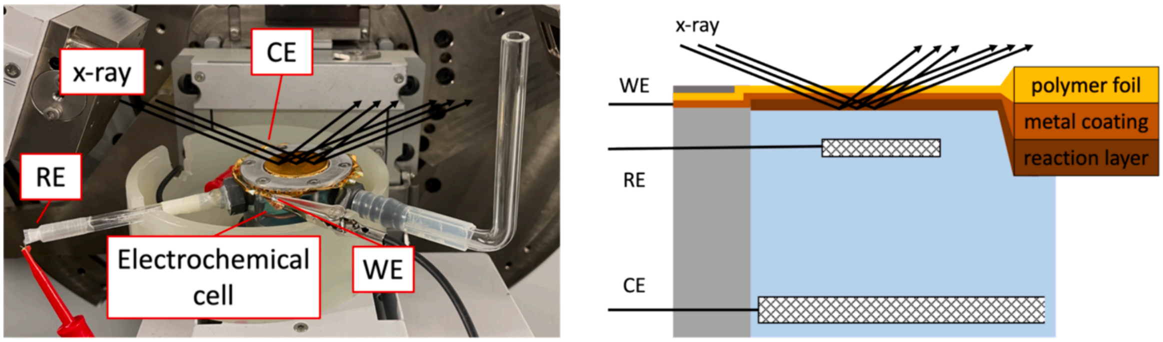

Fig. 3. Left: Experimental measurement setup of the *in-situ* cell in the X-ray diffractometer including contacting of the electrodes; Right: Schematic side view of the measurement setup.

Furthermore, at current densities lower than 1 mA cm^{-2}, the preferred orientation of cuprous oxide is (1 0 0) direction [6]. The intensity of the reflection peaks can serve as a basis for estimating the substance quantity. Data acquisition is facilitated by using the Data-Collector software from PANalytical. The data evaluation and comparative analysis are performed using the HighScore Plus program in conjunction with existing diffraction patterns.

As mentioned, the measuring cell is equipped with two openings to accommodate a pump system and control mass transport. In normal operation mode, electrolyte solution flows through the cell. It is possible to circulate the electrolyte continuously by utilizing a pair of tubes, an external reservoir of solution, and a pump. Moreover, the electrolyte solution can be adjusted to a desired temperature, influencing the deposited grains' size. It is noteworthy, that the deposition kinetics remain linear and independent of temperature [15]. In our case, the available peristaltic pump and its intermittent operation results in periodic deflection of the polymer film and, therefore, a periodic height error for the diffractogram would be observed. This problem is reduced by using a parallel beam mirror on the X-ray source side and a collimator on the detector side. Here, height errors do not have detectable influence on the position of the reflexes but a small influence on the intensity. To avoid this complication, a static solution was used. Instead of using two tubes, one of the openings was sealed, and a glass tube was attached to the remaining one. This glass tube is filled with the electrolyte horizontally a few millimeters above the Mylar® film, allowing a small hydro-static pressure to press the solution against the working electrode surface. This design ensures that the working electrode remains in continuous contact with the electrolyte solution. In this setup without flow-through, the height of the Mylar® film was constant and was perfectly adjusted with respect to the beam pathway before the start of the measurement. As the film was stretched tightly during assembly, similar to the membrane of a drum, the film has no significant curvature that could otherwise have an influence on the peak position, intensity or the width of the reflex. Initial air bubbles within the measuring cell can be prevented through careful filling of the cell. The geometry of the counter electrode, consisting of copper, is designed to exhibit high symmetry to the working electrode. This copper electrode functions as a soluble anode, preventing oxygen evolution, which may collect under the working electrode or other potential side reactions within the lactic acid solution and depletion of copper ions in the electrolyte solution. Possible gas evolution could easily be detected as it would cause a visible change of the filling level in the glass tube.

To enable the copper oxide deposition on the working electrode, a source of copper must be provided. For this purpose, an electrolyte solution with 0.4 M copper sulfate and 3 M lactic acid as the deposition solution is prepared. As galvanostatic deposition of cuprous oxide is only possible at high pH, the pH of the electrolyte solution is adjusted by adding 4 M NaOH to a pH of 13. The doubly charged copper ion is complexed by lactate ions and stays in solution.

During XDR diffractograms measurement-current was paused to provide satisfactory and demonstrable measurements. However, it is possible to perform the *in-situ* method as an *in-operando* method by varying the process parameters. For this purpose, the measurement time of the diffractograms must be shortened, for example by using an image plate detector for a faster acquisition of the intended 2θ range.

4. Results and discussion

4.1. Current density distribution and voltage drop

Calculations of the influence of the sheet resistance on current density distribution and on voltage drop were made for a 1 μm Cu layer. The sheet resistance of this film is $R_{\square} = 0.0244\ \Omega$. The conductivity of the solution taken for the calculation, is about $\sigma = 0.42$ S cm^{-1}.

For the calculation an average current density of 0.2 mA cm^{-2} was assumed, which is close to the experimental conditions. Fig. 4 shows that the voltage drop from the edge contact to the center of the metal film is less than 2 μV. The current density at the edge is about 0.053 % higher than the average of 0.2 mA cm^{-2}. In the center, the current density is about 0.03 % lower than the average. These results prove excellent conditions for a homogeneous distribution of electrochemical reactions across the surface of the working electrode. It shows that either much higher current densities could be applied without significant adverse effects, or thinner metal films could be used as working electrode / current collector for even lower absorption of X-rays, which would allow lower incidence angles.

4.2. Cathodic deposition of Cu_2O

The quantity of deposited copper oxide, or the uniform rate of thickness growth, is determined by using Faraday's law of deposition,

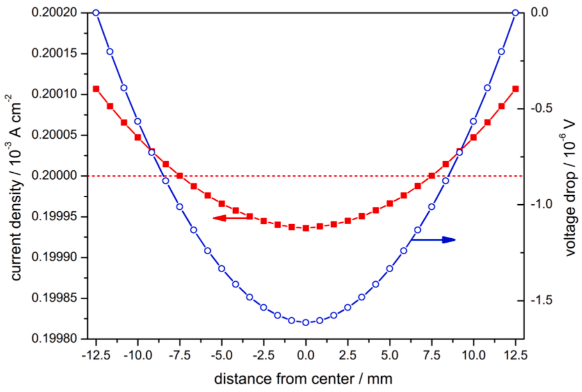

Fig. 4. Simulation results for the current density distribution (filled rectangles) and the potential distribution (open circles) across the working electrode surface. The dotted horizontal line indicates the average current density.

which directly allows the calculation of the nominal layer thickness (Eq. (2)).

$$d = \frac{M \cdot I \cdot t}{z \cdot A \cdot \rho \cdot F} \tag{2}$$

With M as the molecular mass of the deposition substance (143.09 g mol^{-1} for Cu_2O), I the deposition current, t the deposition time in s, z the number of participating electrons in the electrodeposition ($z = 2$ for the reduction of 2 Cu^{2+} to 2 Cu^{+} needed for the formation of Cu_2O), A the area of the working electrode (4.91 cm^2), ρ the density (6.0 g cm^{-3} for Cu_2O) and F the Faraday constant (96485 A s mol^{-1}). According to existing literature, the deposition rate remains constant at thicknesses under 3.5 μm. Additionally, the deposition rate is directly proportional to the deposition current, resulting from Faraday's law [22]. In galvanostatic operation, it is feasible to deposit highly uniform layers up to a thickness of 5.5 μm. Achieving uniform coatings with greater thicknesses requires lower current densities, typically below 0.69 mA cm^{-2} [23]. Working with lower current densities, we can assume a consistent and homogeneous deposition rate.

Using the underlying equation, it is possible to calculate the time required to deposit the desired amount of cuprous oxide. In this work intervals that correspond to 100 nm thin layers were chosen. By Faraday's law, applying 1 mA cathodic for 397.5 s results in 100 nm cuprous oxide deposition on polymer foil. The application of 1 mA implicates a current density of 0.204 mA cm^{-2} at the working electrode.

Various electrochemical measurements are carried out and X-ray diffractograms are recorded *in-situ* to demonstrate the functionality of the designed cell. Fig. 5 displays the background diffractograms over the full 2θ range for the empty cell with 500 nm copper film on the Mylar® foil, filled with distilled water and filled with the electrolyte without applying any current. In case of the cell filled with electrolyte solution a small peak is observed between 2θ values of 36.1–37.3° corresponding to the formation of Cu_2O(1 1 1). In addition, the peak height for Cu(1 1 1) decreases slightly which indicates some corrosion of the copper film during the exposition to the solution. The driving counter reaction could be the oxygen in the solution, because no protective gas flow was applied to avoid gas bubble formation. In the full electrolyte formulation, a solid Cu_2O layer is preferentially obtained because Cu^{2+} ions are complexed by the lactate ions and stay in solution even at higher pH values. This phenomenon was also observed in the deposition experiments which led to an offset for the quantitative determination of the layer thickness.

The following graphic (Fig. 6) illustrates the overlapping diffractograms of a sample corresponding to a deposited Cu_2O layer with a final thickness of 1 μm. Each diffractogram equals a deposition of 100 nm, starting with no current applied. The highlighted region represents the angles of the Cu_2O-peak with (1 1 1) orientation. This peak served as a reference to monitor the growth of the oxide layer. Through this growth, quantitative information is obtained. As evident, only the intensity of this peak increases. The other peak in the diffractogram, between 42 and 45°, which is assigned to Cu, slightly changes due to the corrosion of copper.

Fig. 7 depicts the XRD data of two measurement series corresponding from 1 to 1.5 μm Cu_2O layers in steps of 100 nm. To determine the amount of cuprous oxide the Cu_2O-peak is used as a reference. The counts between 2θ values of 36.1–37.3° are integrated and the background from all measured values is subtracted. In the figure the two measurement series are pictured as circles and crosses. The dashed line represents the theoretical layer thickness for a galvanostatic deposition

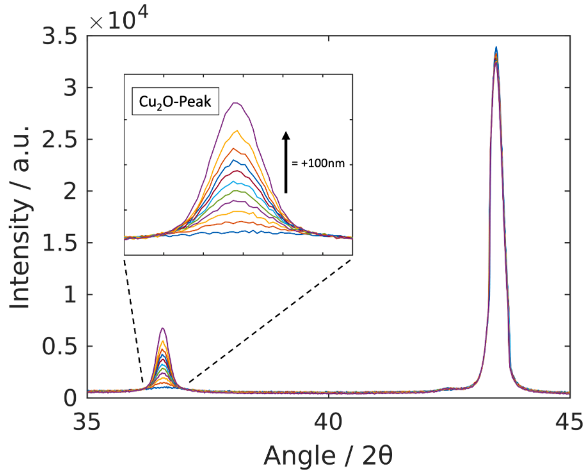

Fig. 6. Illustration of the Cu_2O-peak growth with overlapping diffractograms of selected measurements.

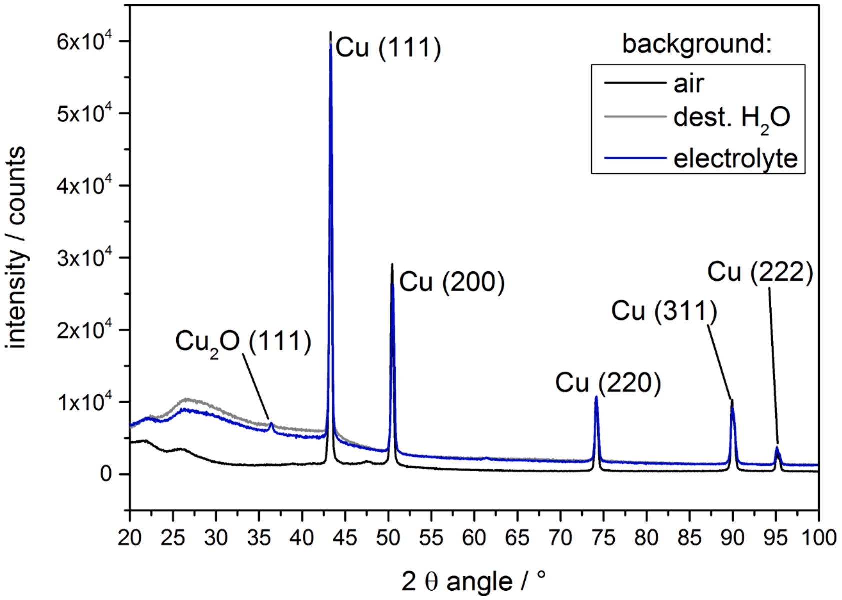

Fig. 5. Comparison of the background diffractograms over the full 2θ range of the cell without applied current for the empty cell, the cell filled with distilled water and filled with electrolyte.

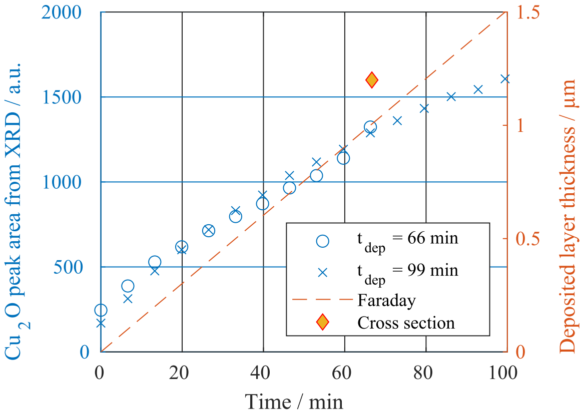

Fig. 7. Results of the diffractograms. The electrochemical measurements are portrayed as points and crosses for different deposition times. The dashed line represents the theoretical layer thickness calculated by Faraday's law. The filled diamond indicates the layer thickness determined by cross section with a scanning electron microscope.

experiment according to Faraday's law. Assuming a current yield of 100 %, a Cu_2O layer is expected to grow linearly with time.

The deviation at the abscissa originates from the natural oxide layer on the working electrode measured in the diffractograms. For low deposition times, the graph demonstrates the linear deposition rate expected from the calculation. At larger times the peak areas deviate from the linear relationship since with the increase of the thickness of Cu_2O, it reaches values in the range of the beam penetration depth. Furthermore, the integrated red diamond depicts the value for the cross section at which the average layer thickness is measured under a scanning electron microscope for the sample corresponding to 1 µm Cu_2O (see Section 4.3). Considering the initial existing cuprous oxide layer the results are well in line with each other.

The cell has demonstrated the capability to conduct electrochemical experiments simultaneously with X-ray diffraction experiments. The *in-situ* GI-XRD technique not only enables qualitative observation but also provides quantitative conclusions. The applied current controls the quantitative aspect, where XRD measurements provide a qualitative validation tool.

In addition, no gas evolution was observed during the measurements, indicating the absence of possible side reactions and a sufficiently large capacity of the electrolyte volume. Consequently, a high current efficiency for oxide formation can be assumed. All flowing electronic charges contribute to the deposition of cuprous oxide, proving that the absence of solution stirring is of minor significance.

4.3. *Measurement of layer thickness*

To verify the layer thickness one selected sample was examined in detail under the scanning electron microscope (SEM). Three various sample preparations were employed: (I) the creation of a microtome section of the film, (II) classic metallographic embedding and polishing, and (III) a focused ion beam (FIB) cutting. The results are depicted in Fig. 8.

In all SEM images, the copper substrate layer is positioned at the bottom, with the deposited copper oxide layer above it. It seems by microtome sectioning, the oxide layer experiences breakage during cutting, likely due to its inherent brittleness. Additionally, the copper layer is divided into two distinct regions: a uniform zone closer to the Mylar® film at the bottom and a porous columnar zone at the top.

In comparison, the classical metallographic method reveals a less fractured oxide layer without distinguishable structures. The dimensions are slightly different, appearing somewhat uneven due to potentially smearing of the soft copper.

To achieve more detailed images, a further attempt was made with FIB cutting. In this case, the two zones in the copper layer are once again visible, although the contrast is lower as in the microtome section. Here, as expected, the deposited copper oxide layer has a homogeneous appearance. The tilt corrected layer thickness correspond to 1.22 µm. This agrees well with the microtome sectioning and in general confirms the validity of the measurements. All three preparation methods provide similar results for different locations on the entire surface. This shows the advantage of our in-situ cell with its homogeneous current density distribution and the resulting homogeneous deposition of the layer.

The deviation to the 1 µm thick cuprous oxide layer calculated can be explained by a naturally built oxide film. As seen in the diffractograms an initial cuprous oxide species was recorded, primarily originating from contact with the atmosphere and electrolyte solution. To inhibit the formation, contact with the atmosphere must be avoided and oxygen free electrolyte solution must be used. Considering the signal intensities before any current is applied, an initial oxide layer of approximately 0.18 µm is present. The difference is calculated by integrating the counts prior to all electrochemical measurements and determine its relative thickness to the following measurements. If this initial oxide layer is taken into account, an electrodeposited layer of 1.04 µm is obtained for the electrochemical measurements. This corresponds to a relative deviation from the theoretically calculated layer thickness of 4 percent.

Furthermore, the composition of the two layers is analyzed using Energy-Dispersive X-ray (EDX) analysis. The copper substrate contains 11.9 at.% oxygen, possibly resulting from the oxidation of the copper over time between sample preparation and measurement. This is a further indication of the presence of an initial naturally occurring oxide layer. As expected, the deposited cuprous oxide layer comprises 35.2 at.% oxygen and 63.7 at.% copper. A minimal amount of 1.1 at.% sulfur is detected, likely residual from the electrolyte solution.

5. Conclusion

In conclusion, we have proposed and characterized a versatile *in-situ* XRD cell design for electrochemical experiments, addressing limitations encountered in conventional setups. By employing a thin metal film

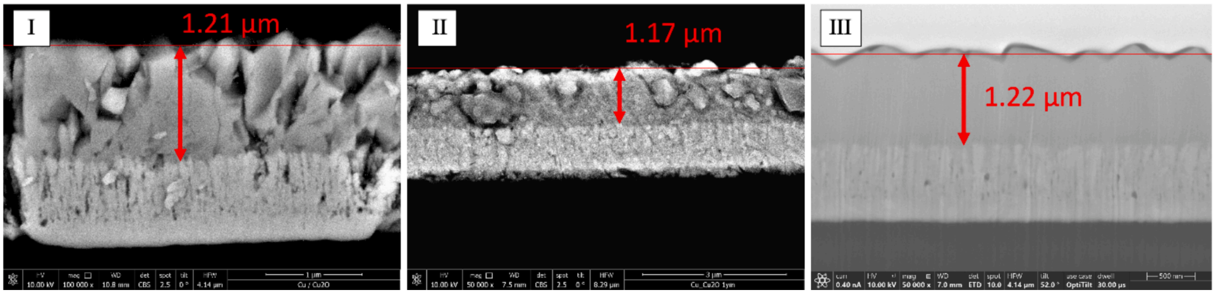

Fig. 8. SEM images of the cross section of a Cu_2O layer prepared by I – microtome preparation; II – embedding and polishing; III FIB cutting. The layer thickness shown in the measurement from number III is the tilt corrected value: $d = 0.96\ \mu m/\sin(52^\circ) = 1.22\ \mu m$.

working electrode on a polymer foil in a backside-illuminated GI-XRD geometry, we have effectively mitigated the issues associated with signal attenuation by electrolyte solution interference. Our cell design facilitates high intensity X-ray signals, enabling precise structural analysis of electrode/electrolyte interfaces.

Through a comprehensive investigation, focusing on the cathodic deposition of Cu_2O, we have demonstrated the functionality and performance of the designed cell. Both the *in-situ* XRD measurements and the SEM images agree well with the layer thickness calculated by Faraday's law. The presented data verify the flawless application. It is shown that qualitative structural information can be obtained from XRD measurements on the one hand and quantitative information from the amount of converted charge on the other. The results are promising and confirm the proper functionality of our approach to investigate electrochemical processes *in-situ*.

Furthermore, our cell design offers distinct advantages, including customizable geometry, homogeneous and high current densities, and the ability to control electrolyte volume and convection. Problems with possible gas development as a side reaction could be solved by tilting the working electrode downwards or to the side with suitable XRD instruments.

In summary, our work presents an easily accessible *in-situ* or even *in-operando* XRD technique for studying electrochemical processes, which provides researchers a tool to gain deeper insights into fundamental mechanisms occurring directly at electrode/electrolyte interfaces.

CRediT authorship contribution statement

Fabian Froech: Writing – original draft, Visualization, Investigation, Formal analysis. **Sabine Kubicek:** Writing – review & editing, Methodology, Investigation, Formal analysis. **Werner Artner:** Writing – review & editing, Investigation. **Michael Nelhiebel:** Writing – review & editing, Funding acquisition. **Silvia Larisegger:** Writing – review & editing, Project administration. **Guenter Fafilek:** Conceptualization, Methodology, Supervision, Validation, Writing – original draft, Writing – review & editing.

Declaration of competing interest

The authors declare that they have no known competing financial interests or personal relationships that could have appeared to influence the work reported in this paper.

Acknowledgements

The preparation of the samples by the Institute for Solid State Physics (C. Eisenmenger-Sittner, TU Wien, Wiedner Hauptstraße 8-10, 1040 Wien, Austria) is gratefully acknowledged. The University Service Facility for Transmission Electron Microscopy (USTEM) provided microtome and FIB cutting and SEM images. The authors acknowledge TU Wien Bibliothek for financial support through its Open Access Funding Program.

References

[1] O.M. Magnussen, J. Drnec, C. Qiu, I. Martens, J.J. Huang, R. Chattot, A. Singer, In situ and operando X-ray scattering methods in electrochemistry and electrocatalysis, Chem. Rev. (2024).

[2] Z. Nagy, H. You, Applications of surface X-ray scattering to electrochemistry problems, Electrochim. Acta 47 (19) (2002) 3037–3055.

[3] D. Stevens, J. Dahn, An in situ small-angle X-ray scattering study of sodium insertion into a nanoporous carbon anode material within an operating electrochemical cell, J. Electrochem. Soc. 147 (12) (2000) 4428.

[4] C. Prehal, A. Samojlov, M. Nachtnebel, L. Lovicar, M. Kriechbaum, H. Amenitsch, S.A. Freunberger, In situ small-angle X-ray scattering reveals solution phase discharge of Li–O2 batteries with weakly solvating electrolytes, Proc. Natl. Acad. Sci. 118 (14) (2021) e2021893118.

[5] R. Kara, H. Lahmar, L. Mentar, R. Siab, F. Kadirgan, A. Azizi, Electrochemical growth and characterization of Cu2O: Na/ZnO heterojunctions for solar cells applications, J. Alloys Compd. 817 (2020) 152748.

[6] T. Shinagawa, Y. Ida, K. Mizuno, S. Watase, M. Watanabe, M. Inaba, A. Tasaka, M. Izaki, Controllable growth orientation of Ag2O and Cu2O films by electrocrystallization from aqueous solutions, Cryst. Growth Des. 13 (1) (2013) 52–58.

[7] NIST, X-ray Mass Attenuation Coefficients, Water, https://physics.nist.gov/PhysRefData/XrayMassCoef/ComTab/water.html (accessed Apr. 9 2024).

[8] M. Fleischmann, A. Oliver, J. Robinson, In situ x-ray diffraction studies of electrode solution interfaces, Electrochim. Acta 31 (8) (1986) 899–906.

[9] M.G. Samant, M.F. Toney, G.L. Borges, L. Blum, O.R. Melroy, In-situ grazing incidence X-ray diffraction study of electrochemically deposited Pb monolayers on Ag (111), Surf. Sci. 193 (1–2) (1988) L29–L36.

[10] J.-P. Veder, A. Nafady, G. Clarke, R.P. Williams, R. De Marco, A.M. Bond, A flow cell for transient voltammetry and in situ grazing incidence X-ray diffraction characterization of electrocrystallized cadmium (II) tetracyanoquinodimethane, Electrochim. Acta 56 (3) (2011) 1546–1553.

[11] M. Imafuku, M. Kurosaki, K. Kawasaki, Development of an in-situ X-ray diffraction system for observation of electrodeposition of metallic layers, J. Synchrotron Radiat. 5 (3) (1998) 935–936.

[12] M. Ndjeri, S. Peulon, M. Schlegel, A. Chaussé, In situ grazing-incidence X-ray diffraction during electrodeposition of birnessite thin films: identification of solid precursors, Electrochem. Commun. 13 (5) (2011) 491–494.

[13] E. Meulenkamp, An electrochemical cell for simultaneous in situ X-ray diffraction and optical measurements, J. Electrochem. Soc. 145 (8) (1998) 2759.

[14] S. Reither, W. Artner, A. Eder, S. Larisegger, M. Nelhiebel, C. Eisenmenger-Sittner, G. Fafilek, On the in-situ grazing incidence X-ray diffraction of electrochemically formed thin films, ECS Trans. 80 (10) (2017) 1231.

[15] T. Mahalingam, J. Chitra, S. Rajendran, M. Jayachandran, M.J. Chockalingam, Galvanostatic deposition and characterization of cuprous oxide thin films, J. Cryst. Growth 216 (1–4) (2000) 304–310.

[16] N.G. Elfadill, M. Hashim, K.M. Chahrour, S. Mohammed, Preparation of p-type Na-doped Cu2O by electrodeposition for a pn homojunction thin film solar cell, Semicond. Sci. Technol. 31 (6) (2016) 065001.

[17] K. Mairhofer, B. Kipper-Pires, G. Leitner, G. Fafilek, Photoassisted electrodeposition of cuprous oxide thin films, ECS Trans. 105 (1) (2021) 441.

[18] E. Achilli, A. Vertova, A. Visibile, C. Locatelli, A. Minguzzi, S. Rondinini, P. Ghigna, Structure and stability of a copper (II) lactate complex in alkaline solution: a case study by energy-dispersive X-ray absorption spectroscopy, Inorg. Chem. 56 (12) (2017) 6982–6989.

[19] A.A. Hssi, L. Atourki, N. Labchir, M. Ouafi, K. Abouabassi, A. Elfanaoui, A. Ihlal, K. Bouabid, Optical and dielectric properties of electrochemically deposited p-Cu2O films, Mater. Res. Express 7 (1) (2020) 016424.

[20] M. Pourbaix, Atlas of Electrochemical Equilibria in Aqueous Solutions, National Association of Corrosion Engineers, 1974.

[21] A.D. Inc., LTspice®, https://www.analog.com/en/resources/design-tools-and-calculators/ltspice-simulator.html (accessed Feb. 19 2024).

[22] A. Rakhshani, A. Al-Jassar, J. Varghese, Electrodeposition and characterization of cuprous oxide, Thin Solid Films 148 (2) (1987) 191–201.

[23] A. Rakhshani, J. Varghese, Galvanostatic deposition of thin films of cuprous oxide, Solar Energy Mater. 15 (4) (1987) 237–248.